Complex magnetism in Ni3TeO6-type Co3TeO6 and high-pressure polymorphs of Mn3-xCoxTeO6 solid solutions

Journal Name

COMMUNICATION

Complex magnetism in Ni_3TeO_6-type Co_3TeO_6 and high-pressure polymorphs of $Mn_{3-x}Co_xTeO_6$ solid solutions.

Received 00th January 20xx,
Accepted 00th January 20xx

DOI: 10.1039/x0xx00000x

www.rsc.org/

Elena Solana-Madruga,[a,b,*] Cintli Aguilar-Maldonado,[a] Clemens Ritter,[c] Marielle Huvé[a], Olivier Mentré[a] J. Paul Attfield[b] and Ángel M. Arévalo-López[a*].

New Ni_3TeO_6-type (NTO) and double perovskite (DPv) polymorphs of Co_3TeO_6 are synthesised at pressures of 15 GPa. A complex elliptic helical magnetic order is observed in the NTO polymorph (T_{N1} = 58 K) that reorientates (42 K) and further splits (T_{N2} = 23.5 K) creating a coexisting helix. Increasing Co content within the $Mn_{3-x}Co_xTeO_6$ system changes the dominant DPv phase to NTO structural type and drastically modifies the magnetic behaviour. DPv Co_3TeO_6 is the first A-site double cobaltite.

High-pressure and high-temperature synthesis has proven to be of wide interest in the search for new materials with notable properties such as multiferrocity. A-site ABO_3 and related manganites are able to crystallise in perovskite and corundum related structures with varied magnetic and electrical properties. For instance, localized d^5 (Mn^{2+}) and itinerant d^1 electrons (V^{4+}) coexist in $MnVO_3$.[1] High pressure $Mn_2BB'O_6$ double perovskites (DPvs) show a plethora of magnetic behaviours, with simple antiferromagnetic (AFM),[2-5] collinear,[6] perpendicular[7] and continuously rotating ferrimagnetic structures[8] and more complex incommensurate-elliptical helices.[9]

The stacking of honeycomb / triangular magnetic sublattices in ordered-corundum structures such as Ni_3TeO_6-type (NTO), induces a strong magnetic frustration, usually resulting in the formation of incommensurate helical magnetic structures,[10] sometimes with thermal dependence and lock-in of their propagation vector[2] at low temperatures.[11]

Ambient pressure M_3TeO_6 (M = Mn and Co) phases crystallise in distorted corundum-based structures, also showing complex magnetic behaviours. Mn_3TeO_6-I (*R-3*) shows an elliptical helix and a sinusoidal spin density wave coexisting below 24 K.[12] It also shows multiferroic properties below 21 K.[13] Co_3TeO_6-I (*C2/c*) has 5 independent Co sites, providing a rich magnetic phase diagram[14,15] with subsequent magnetic transitions originating an incommensurate [0 k_y k_z], a [0 0 0] (k_0 from here) and a sinusoidal [0 ½ ¼] magnetic structures.[16] It is also notable for showing a magnetic field-induced electrical polarisation.[17,18]

The high-pressure DPv modification of Mn_3TeO_6 (Mn_2MnTeO_6-II, *P2₁/n*), was recently reported as a collinear AFM with k = [½ 0 ½] below 36 K with an unusually large frustration index of 5.1 due to the rock-salt order of the d^5 Mn^{2+} cations with the diamagnetic d^{10} Te^{6+}.[3] In this communication, we report the high-pressure phase modification of Co_3TeO_6 (HP-Co_3TeO_6) and its combination with DPv-Mn_3TeO_6 into the HP-$Mn_{3-x}Co_xTeO_6$ series. Co_3TeO_6 presents both NTO- and DPv-type structures from high pressure-high temperature synthesis, with predominance of NTO at the applied 15 GPa synthesis pressure and evidence of higher stability of the denser DPv polymorph as a function of pressure. The NTO polymorph shows an incommensurate elliptical helix below 58 K. The magnetic propagation vector shifts with temperature and locks at 23 K, where it splits creating a coexisting circular helix. Dealing with the mixed Mn/Co compounds, the NTO-type structure is retained for Co-rich members but changes to DPv polymorph at the Mn-rich side of the system. The presence of small proportions of either Mn^{2+} (d^5, S = 5/2) or Co^{2+} (d^7, S = 3/2) cations induces dramatic magnetic changes, reflecting the essential role of t_{2g} orbitals in the set of magnetic exchanges.

HP-$Mn_{3-x}Co_xTeO_6$ samples were prepared for x = 0.5, 1, 1.5, 2, 2.5 and 3 by high-pressure high-temperature phase transformation at 8, 10, 10, 12, 13 and 15 GPa respectively as detailed in ESI. Note that higher pressures are needed to stabilise larger amounts of smaller Co^{2+} in the same polymorph (0.90 and 0.745 Å vs. 0.96 and 0.83 Å for Mn^{2+} in 8- and 6- fold coordination).[19]

[a] Univ. Lille, CNRS, Centrale Lille, ENSCL, Univ. Artois, UMR 8181 - UCCS - Unité de Catalyse et Chimie du Solide, F-59000 Lille, France. * elena.solanamadruga@univ-lille.fr and angel.arevalo-lopez@univ-lille.fr
[b] Centre for Science at Extreme Conditions (CSEC) and School of Chemistry, The University of Edinburgh. EH9 3FD, U.K.
[c] Institut Laue-Langevin, Avenue des Martyrs 71, 32042, Grenoble Cedex, France.

‡ Electronic Supplementary Information (ESI) available: supporting figures and tables. See DOI: 10.1039/x0xx00000x

Site	x	Y	z	B_{iso}(Å^2)	Occ
Co1 (3a)	0.0	0.0	0.062[a]	0.21(7)	1.0
Co2 (3a)	0.0	0.0	0.264(2)	0.21*	1.0
Co3 (3a)	0.0	0.0	0.540(3)	0.21*	1.0
Te (3a)	0.0	0.0	0.765(2)	0.21*	1.0
O1 (9b)	0.337(1)	0.040(1)	0.169(2)	0.9(2)	1.0
O2 (9b)	0.329(1)	0.367(1)	0.337(2)	0.1(1)	1.0
3x d_{Co1-O1} (Å)	2.21(2)		3x d_{Co3-O1} (Å)	2.00(1)	
3x d_{Co1-O2} (Å)	2.02(1)		3x d_{Co3-O2} (Å)	2.37(5)	
3x d_{Co2-O1} (Å)	2.11(3)		3x d_{Te-O1} (Å)	1.89(3)	
3x d_{Co2-O2} (Å)	2.07(3)		3x d_{Te-O2} (Å)	2.02(4)	
$\Delta Co1*10^3$	2.02 [b]		$\Delta Co3*10^3$	7.17 [b]	
$\Delta Co2*10^3$	0.09 [b]		$\Delta Te*10^3$	1.11 [b]	
BVS_{Co1}	1.98		BVS_{Co3}	1.80	
BVS_{Co2}	2.04		BVS_{Te}	5.45	

Table 1. Atomic positions and main interatomic distances and angles from the Rietveld fit of NTO-Co_3TeO_6 against 300 K NPD data. S.G. *R3*, *a* = 5.1874(2) Å, *c* = 13.8015(7) Å.
[a] Co1 site is used as the refence for the cell. [b] Δ values calculated from $(1/6)*\sum[(d_i-d_{av})/d_{av}]^2$.* Constrained to Co1.

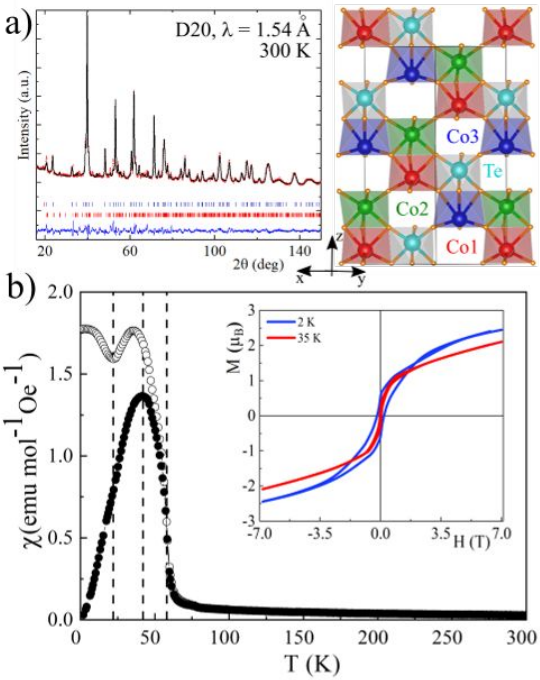

Fig. 1. a) Rietveld fit of the 300 K NPD data for HP-Co_3TeO_6. First and second row of Bragg tick marks refer to 85.5% of NTO- and 14.5 % of DPv-polymorphs (see text). NTO-type structure shown on the right panel. b) FC-ZFC magnetic susceptibility curves, shown as open and closed circles respectively. Vertical broken lines mark transitions observed in the NPD data. Inset shows magnetisation-field loops.

The NTO-type Co_3TeO_6 structure has been refined from 300 K high-resolution NPD data (λ = 1.54 Å) collected at D20 at ILL. Rietveld fit results reveal a fully ordered NTO-type structure with four independent cation sites (S.G. *R3*); see Figure 1a and Table 1. It consists of alternated *ab* honeycomb layers of $Co1O_6/TeO_6$ ($Co2O_6/Co3O_6$) edge sharing octahedra.

Together, it forms $Co1O_6/Co2O_6$ ($Co3O_6/TeO_6$) face sharing dimers along *c* and $Co1O_6/Co3O_6$ corner sharing along the [012] direction. Octahedral distortions, calculated from Δ = $(1/6)*\sum[(d_i-d_{av})/d_{av}]^2$, reveal the highest distortion for $Co3O_6$ ($7.17*10^{-3}$) due to its Coulomb repulsions against the faced non-polarisable d^{10} Te^{6+} cation. Such distortion is cushioned in the Co1-Co2 dimer. Bond Valence Sum calculations confirm the 2+ and 6+ oxidation states for Co and Te in all sites, and thus the nominal $Co^{2+}{}_3Te^{6+}O_6$ stoichiometry. The presence of a possible superstructure or any short-range order for NTO-Co_3TeO_6 was checked and ruled out by means of transmission electron microscopy (ESI). Evidence of an even higher-pressure Co_3TeO_6 polymorph with DPv structure similar to that of Mn_3TeO_6-II was observed and considered in the refinement and discussed below. The existence of both NTO and DPv phases throughout the HP-$Mn_{3-x}Co_xTeO_6$ series suggest the possibility to quench both phases under different synthesis conditions. However, DPv → NTO phase transition at decompression may be possible, as observed in $ScFeO_3$,[20] and cannot be discarded. In-situ HP diffraction studies would clarify this matter.

Figure 1b shows the bulk magnetic behaviour of HP-Co_3TeO_6. The Curie-Weiss fit to the inverse susceptibility results in θ = -73 K and μ_{eff} = 5.3 μ_B / Co^{2+}, showing a large contribution of spin orbit coupling (SOC) and predominant AFM interactions. FC-ZFC susceptibility curves show a first transition at T_{N1} = 58 K, a maximum at 42 K (increase of the reorientation as discussed below) and a second transition at T_{N2} = 23.5 K. Hysteresis loops in the inset of Fig. 1b confirm the presence of a ferromagnetic component of ~ 1 μ_B at 35 K with hysteretic behaviour at 2 K. The presence of minor (14.5%) AFM DPv HP phase with lower T_N is masked by the bulk (ferri)magnetic behaviour of the main NTO phase. The unambiguous identification of both polymorphs from SXRD and NPD along with the stability of the refinements against all NPD data sets and difference patterns confirms the feasibility of the magnetic models discussed below.

Low temperature NPD data for HP-Co_3TeO_6 sample are shown in Figure 2. The magnetic peaks at 40 K can be indexed with coexisting propagation vectors k_{z1} = [0 0 0.2213(6)] and k_0 = [0 0 0]. The presence of the main (003) magnetic and satellite peaks indicates that spins are mainly perpendicular to the *c* axis for both k vectors. Their combination could signify coexistence of a collinear and a helical magnetic structure. However, the simultaneous appearance of both sets of magnetic peaks for all NTO-type HP-$Mn_{3-x}Co_xTeO_6$ compounds suggests a single magnetic phase. The combination of collinear and helical spin structures modulates the magnetic moments in the *ab* plane, giving rise to an elliptical helix.

The evolution of k_{z1} upon cooling shows its splitting at T_{N2} into k_{z1} and k_{z2}, both vectors freezing at 16 K with refined

values of k_{z1} = 0.3988(9) and k_{z2} = 0.4742(8) at 1.5 K, see Figure 2.

The magnetic structures were refined against NPD difference patterns 40 K – 80 K (k_{z1}+k_0) and 1.5 K – 80 K (k_{z1}+k_0, k_{z2}), see ESI for details. The elliptical helix at 40 K (R_{mag} = 8.70 %) presents modulated magnetic moments within the *ab* plane varying between 0.48(1) and 2.44(1) μ_B. One magnetic layer is projected along [001] in Fig. 3a (top). The fit of the 1.5 K – 80 K difference pattern reveals the contribution of the k_0 vector only to k_{z1} phase, while the new k_{z2} phase has pure helical topology. The magnetic moments in each of the helical phases (following each incommensurate k vector) were constrained to the same values for stability of the refinements. The lowest temperature fit results in maximum values of 2.87(1) μ_B, the modulated moment of the elliptical phase increasing from 0.98(1) μ_B. The phase proportion from this fit refines to 56 % elliptical and 44 % circular helices, with magnetic reliability factors R_{mag} = 2.18 % and 3.28 % respectively.

Figure 2b (top) shows the thermal evolution of the maximum magnetic moment in the elliptical phase, equal to the total magnetic moment in the circular helix. The fit to the critical law $\mu_{(T)} = \mu_{(0)} * [1 -(T/T_{N1})]^{\beta}$ in the $(T_{N1}/2) < T < T_{N1}$ temperature range results in T_{N1} = 58.7(3) K, $\mu_{(0)}$ = 3.04(9) μ_B, in good agreement with the expected value for S = 3/2 high spin Co^{2+} cations, and β = 0.22(2), confirming the magnetic 2D-XY behaviour. The DPv-Co_3TeO_6 minor phase was included in the magnetic refinements using k = [½ 0 ½] similar to that of Mn_3TeO_6-II. Further studies will be addressed to the full magnetic characterisation of this DPv polymorph as a pure phase.

The spin angles between Co1-Co2/Co2-Co3 sites at 1.5 K are -133(1)°/179(1)° and -172(1)°/154(1)° for the elliptical and circular helices respectively. The nearly ideal 180° AFM and the ~120° angle, often stabilised in frustrated trigonal compounds, reflects the strong competition of the involved interactions (see below) and justifies the low temperature separation into two coexisting magnetic phases.

Other possible driving forces could be local strains or minor chemical disorder effects (e.g. local Co/Te antisites) too small to be detected. At least dealing with a phase segregation at the microscopic scale, a sensitive decrease of magnetic correlation lengths is expected across T_{N2}. Such correlation change was checked by the broadening of magnetic satellites in $\Delta L \sim 150$ nm, as calculated using the Scherrer formula.

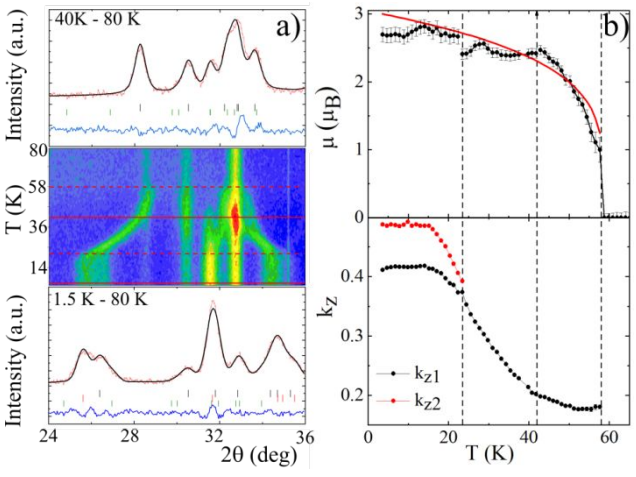

Figure 2. a) Rietveld fits of the HP-Co_3TeO_6 NPD 40 K – 80 K (top) and 1.5 K – 80 K (bottom) difference patterns. Middle panel shows the 2D thermodiffraction, with dashed red lines at T_{N1} and T_{N2} and solid lines for fitted T. b) Thermal evolution of the magnetic moment and k_z vector. Fit to the critical law for the magnetic moments is shown as a red line.

The remarkable magnetic complexity of NTO-Co_3TeO_6, unambiguously intrinsic to the NTO phase according to the stability of all Rietveld fits against our NPD data, has motivated the study of the HP-$Mn_{3-x}Co_xTeO_6$ system. The series shows a coherent evolution, crystallising with the DPv structure for x < 1.5 and with NTO structure for x > 1.5 (ESI). The x = 1.5 intermediate composition shows phase coexistence refined to 88.4 % DPv *vs.* 11.6 % NTO from NPD data collected under high resolution at 300 K. The use of 12-13 GPa could solely drive to the rhombohedral polymorph, while for x = 3 small amounts of DPv (14.5%) are observed when prepared at 15 GPa. This suggests the accessibility to the DPv polymorph for the complete series at higher pressures. DPv-Co_3TeO_6 is remarkable as the first A-site double cobaltite, and further studies will be required to isolate it for a complete characterisation.

The atomic positions, summarised in ESI tables, show full cation order among 2+/6+ B-site cations and site preference for the larger Mn^{2+} at the A sites. Among the NTO phases, cation order/site preference is also observed. The magnetic behaviour of the solid solution shows a coherent evolution in transition temperature and refined magnetic moments at 1.5 K, as summarised in Table 2 and the magnetic phase diagram in Figure 3b. Among the DPv polymorphs, two AFM structures with k = [½ 0 ½] (like that of Mn_3TeO_6-II)[3] and k_0 (Fig. 3c) are observed, both with collinear spins in the *ac* plane. All the NTO phases show coexistence of k_0 and an incommensurate k_z propagation vectors with simultaneous orders, revealing elliptical helix magnetic structures like that of NTO-Co_3TeO_6. Surprisingly, no thermal dependence of k_z was observed for mixed Mn/Co phases (ESI).

Table 2. Magnetic transition temperatures, propagation vectors, effective magnetic moment per M^{2+} (μ_{eff}) from Curie-Weiss fits and refined magnetic moments in A and B sites ($\mu_{A/B}$) for HP-$Mn_{3-x}Co_xTeO_6$ system at 1.5 K. The refined magnetic moments for the NTO phases show the total/maximum value for the k_z phase.

x	T_N (K)	k	DPv/ NTO(%)	μ_{eff} (μ_B)	$\mu_{A/B}$ (μ_B)
0	36	[½ 0 ½]	100	5.6	4.8(6)/3.9(1)
0.5	31 23	[½ 0 ½] [0 0 0]	100	x	3.61(2)/2.42(2) 3.58(1)/2.40(2)
1.0	27	[0 0 0]	100	5.4	3.21(1)/1.84(2)
1.5	25 67	[0 0 0] $k_0 + k_z = 0.080(1)$	88.4(1) 11.6(1)	5.9	3.48(1)/1.25(3) 3.89(4)
2.0	72	$k_0 + k_z = 0.094(1)$	100	5.3	4.47(1)
2.5	66	$k_0 + k_z = 0.117(1)$	100	5.7	4.13(1)

	47	[½ 0 ½]	14.5(1)		
3.0	58	$k_0 + *k_{z1}$ = 0.3988(9)		5.3	2.87(1)
	23	$*k_{z2}$ = 0.4742(8)	85.5(1)		

Expected μ_{eff} = 5.92 μ_B/Mn^{2+} / up to 6.63 μ_B/Co^{2+} considering SOC. [x] Experimental issues prevent CW fit. * T-dependent.

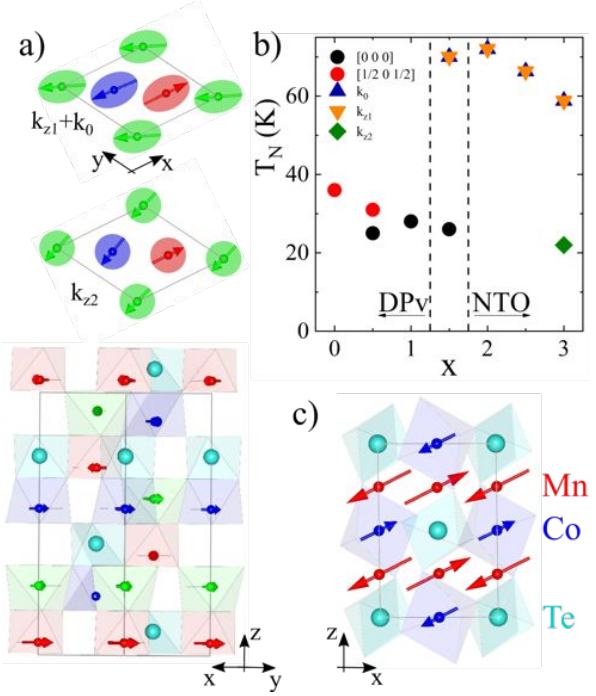

Figure 3. a) [001] projection of the elliptical (top) and circular (middle) magnetic structures of NTO-Co_3TeO_6 at 1.5 K. The bottom panel shows half-cell of the longer k_{z2} phase along [110]. b) Phase diagram for the HP-$Mn_{3-x}Co_xTeO_6$ solid solution c) k_0 magnetic structure of the DPv-Mn_2CoTeO_6.

The cation order and the progressive evolution from d^5 to d^7 weakens the superexchange interactions through oxygen in both polymorphs and more importantly the direct interactions via t_{2g}-t_{2g} orbital overlap in face sharing Co1-Co2 and edge sharing Co2-Co3 sites in the NTO phases. This induces the strongest magnetic frustration for larger Co content, justifying the decreasing T_N and the simple thermal evolution of 1.5 < x < 3 compounds.

In conclusion, a new high pressure Co_3TeO_6 *R3* NTO polymorph has been prepared. Its complex magnetic behaviour is dominated by the strong frustration of the stacked honeycomb and triangular magnetic sublattices. Below 58 K an elliptical helix magnetic structure with temperature dependent k_{z1} vector rotates and splits below 23 K, where it coexists with a k_{z2} circular helix. Evidence for a higher pressure DPv-Co_3TeO_6 with k = [½ 0 ½], notable as the first A-site double cobaltite, will be further studied. The HP-$Mn_{3-x}Co_xTeO_6$ system between NTO-Co_3TeO_6 and Mn_3TeO_6-II has a coherent structural and magnetic evolution from AFM DPv (x < 1.5) to elliptical NTO (x > 1.5). The presence of any Mn^{2+} (d^5, S = 5/2) in the NTO polymorphs prevents the thermal dependence of their incommensurate k_z vector and the presence of any Co^{2+} (d^7, S = 3/2) in the DPv phases changes the k = [½ 0 ½] AFM structure into a different k_0 one.

These dramatic magnetic effects reflect the essential role of t_{2g} orbitals in the magnetic behaviour of these compounds. Recently, Co_3TeO_6 has also been prepared at 5 GPa and their findings agree with our results.[21] However, those authors did not observe nor predict the DPv Co_3TeO_6 higher pressure phase.

We thank EPSRC for support, and Diamond and the ILL for beamtime. Stephen Thompson is acknowledged for assistance on I11 data collection. AMAL thanks the ANR-AMANTS project (19-CE08-0002-01). CAM thanks CONACyT-Mexico for a post-doctoral fellowship (CVU 350841). Chevreul Institute (FR 2638), Region Hauts-de-France, and FEDER for funding the X-ray diffractometers, electron microscope and the PPMS magnetometer.

Conflicts of interest

There are no conflicts of interest to declare.

Notes and references

M. Markkula, A. M. Arévalo-López, A. Kusmartseva, J.A. Rodgers, C. Ritter, H. Wu, J.P. Attfield, *Phys. Rev. B.* 2011, **84**, 094450.
[2] A. J. Dos santos-García, E. Solana-Madruga, C. Ritter, D. Ávila-Brande, O. Fabelo, R. Sáez-Puche, *Dalton Trans.*, 2015, **44**, 10665.
[3] A.M. Arévalo-López, E. Solana-Madruga, C. Aguilar-Maldonado, C. Ritter, O. Mentré, J.P. Attfield, *Chem. Commun.* 2019, **55**, 14470-14473.
[4] C. E. Frank, E. E. McCabe, F. Orlandi, P. Manuel, X. Tan, Z. Deng, M. Croft, V. Cascos, T. Emge, H. L. Feng, S. Lapidus, C. Jin, M. X. Wu, M. R. Li, S. Ehrlich, S. Khalid, N. Quackenbush, S. Yu, D. Walker, M. Greenblatt, *Chem. Commun.* 2019, **55**, 3331-3334.
[5] E. Solana-Madruga, A.J. Dos santos-García, A.M. Arévalo-López, D. Ávila-Brande, C. Ritter, J.P. Attfield, R. Sáez-Puche, *Dalton Trans.*, 2015, **44**, 20441-20448.
[6] A.M. Arévalo-López, G.M. McNally, J.P. Attfield, *Angew. Chem. Int. Ed.* 2015, **54**, 12074.
[7] A. M. Arévalo-López, F. Stegemann, J. P. Attfield, *Chem. Commun.*, 2016, **52**, 5558.
[8] E. Solana-Madruga, K. N. Alharbi, M. Herz, P. Manuel, J. P. Attfield, *Chem. Commun.*, 2020, **56**, 12574-12577.
[9] A. J. Dos santos-García, C. Ritter, E. Solana-Madruga, R. Sáez-Puche, *J. Phys.: Condens. Matter*, 2013, **25**, 206004.
[10] A. J. Dos santos-García, E. Solana-Madruga, C. Ritter, A. Andrada-Chacón, J. Sánchez-Benítez, F. J. Mompean, M. Garcia-Hernandez, R. Sáez-Puche, R. Schmidt, *Angew. Chem. Int. Ed.* 2017, **56**, 4438 –4442.
[11] Á. M. Arévalo-López, E. Solana-Madruga, E. P. Arévalo-López, D. Khalyavin, M. Kepa, A. J. Dos santos-García, R. Sáez-Puche, J. P. Attfield, *Phys. Rev. B,* 2018, **98**, 214403.
[12] L. Zhao, Z. Hu, C.-Y. Kuo, T.-W. Pi, M.-K. Wu, L.H. Tjeng, A.C. Komarek, *Phys. Status Solidi RRL* 2015, **9**, 730.
[13] S.A. Ivanov, C. Ritter, P. Nordblad, R. Tellgren, M. Weil, V. Carolus, T. Lottermoser, M. Fiebig, R. Mathieu, *J. Phys. D: Appl. Phys.* 2017, **50**, 085001.
[14] J.L. Her, C.C. Chou, Y.H. Matsuda, K. Kindo, H. Berger, K.F. Tseng, C.W. Wang, H.D. Yang, *Phys. Rev. B.* 2011, **84**, 235123.
[15] C.-W. Wang, C.-H. Lee, C.-Y. Li, C.-M. Wu, W.-H. Li, C.-C. Chou, H.-D. Yang, J.W. Lynn, Q. Huang, A.B. Harris, H. Berger, *Phys. Rev. B.* 2013, **88**, 184427.
[16] S. A. Ivanov, R. Tellgren, C. Ritter, P. Nordblad, R. Mathieu, G. André, E.D. Politova, M. Weil, *Mat. Res. Bull.* 2012, **47**, 63.
[17] M. Hudl, R. Mathieu, S.A. Ivanov, M. Weil, V. Carolus, T. Lottermoser, M. Fiebig, Y. Tokunaga, Y. Taguchi, Y. Tokura, P. Nordblad, *Phys. Rev. B.* 2011, **84**, 180404(R).
[18] A.B. Harris, *Phys. Rev. B.* 2012, **85**, 100403(R).
[19] R. D. Shannon, C. T. Prewitt, *Acta Cryst. B.* 1969, **25**, 925.

[20] T. Kawamoto, K. Fujita, I. Yamada, T. Matoba, S. J. Kim, P. Gao, X. Pan, S. D. Findlay, C. Tassel, H. Kageyama, J. Hester, T. Irifune, H. Akamatsu, K. Tanaka, *J. Am. Chem. Soc.* 2014, **136**, 15291.
[21] Y. Han, M. Wu, C. Gui, C. Zhu, Z. Sun, M.-H. Zhao, A. A. Savina, A. M. Abakumov, B. Wang, L. H. He, J. Chen, M. Croft, S. Ehrlich, S. Khalid, Z. Deng, C. Jin, C. P. Grams, J. Hemberger, X. Wang, J. Hong, U. Adem, M. Ye, S. Dong, M.-R. Li, *npj Quantum Materials* 2020, **5**, 92.